



Generation and evolution of hydrothermal fluids at Yellowstone: Insights from the Heart Lake Geyser Basin

J. B. Lowenstern and D. Bergfeld

*Volcano Science Center, U.S. Geological Survey, Mail Stop 910, Menlo Park, California 94025, USA
(jlownstern@usgs.gov)*

W. C. Evans and S. Hurwitz

National Research Program, U.S. Geological Survey, Mail Stop 439, Menlo Park, California 94025, USA

[1] We sampled fumaroles and hot springs from the Heart Lake Geyser Basin (HLGB), measured water and gas discharge, and estimated heat and mass flux from this geothermal area in 2009. The combined data set reveals that diverse fluids share an origin by mixing of deep solute-rich parent water with dilute heated meteoric water, accompanied by subsequent boiling. A variety of chemical and isotopic geothermometers are consistent with a parent water that equilibrates with rocks at $205^{\circ}\text{C} \pm 10^{\circ}\text{C}$ and then undergoes $21\% \pm 2\%$ adiabatic boiling. Measured diffuse CO_2 flux and fumarole compositions are consistent with an initial dissolved CO_2 concentration of 21 ± 7 mmol upon arrival at the caldera boundary and prior to southeast flow, boiling, and discharge along the Witch Creek drainage. The calculated advective flow from the basin is 78 ± 16 L s^{-1} of parent thermal water, corresponding to 68 ± 14 MW, or $\sim 1\%$ of the estimated thermal flux from Yellowstone. Helium and carbon isotopes reveal minor addition of locally derived crustal, biogenic, and meteoric gases as this fluid boils and degasses, reducing the He isotope ratio (R_c/R_a) from 2.91 to 1.09. The HLGB is one of the few thermal areas at Yellowstone that approaches a closed system, where a series of progressively boiled waters can be sampled along with related steam and noncondensable gas. At other Yellowstone locations, steam and gas are found without associated neutral Cl waters (e.g., Hot Spring Basin) or Cl-rich waters emerge without significant associated steam and gas (Upper Geyser Basin).

Components: 18,600 words, 11 figures, 3 tables.

Keywords: chlorine; flux; geothermal; noble gas.

Index Terms: 1012 Geochemistry: Reactions and phase equilibria (3612, 8412); 1041 Geochemistry: Stable isotope geochemistry (0454, 4870); 1814 Hydrology: Energy budgets.

Received 15 August 2011; **Revised** 15 December 2011; **Accepted** 20 December 2011; **Published** 28 January 2012.

Lowenstern, J. B., D. Bergfeld, W. C. Evans, and S. Hurwitz (2012), Generation and evolution of hydrothermal fluids at Yellowstone: Insights from the Heart Lake Geyser Basin, *Geochem. Geophys. Geosyst.*, 13, Q01017, doi:10.1029/2011GC003835.

1. Introduction

[2] The Yellowstone hydrothermal system is justifiably famous for its silica-rich sinters and erupting geysers, as well as its acidic, multihued mud pots. The two types of fluids that form these surface features are very different; silica sinter forms where Cl- and silica-rich “neutral Cl” waters emerge, often at some of the lower elevations in the park [Allen and Day, 1935; White *et al.*, 1971; Fournier, 1989; Hearn *et al.*, 1990]. Near pools, the silica precipitates to form sinter terraces, which are sloping plains of amorphous silica that are typically decorated with biological mats of thermophile life forms [Brock, 1978; Braunstein and Lowe, 2001; Guidry and Chafetz, 2003]. Geysers erupt similar waters, either through pools or cone-shaped mounds of knobby geyserite (also amorphous silica). In contrast, mud pots form where fumarolic steam and accompanying sulfur react with local rock to form clay-rich alteration products [Fournier, 1989; Nordstrom *et al.*, 2005; Inskeep *et al.*, 2010]. Related waters contain significant amounts of sulfuric acid with negligible amounts of Cl. Early on, Allen and Day [1935, pp. 508–509] recognized that less water was discharged from acid-altered areas compared with the sinter-forming areas. Moreover, the amount of gas bubbling through acid (often nonflowing) pools is considerably greater than that observed from neutral Cl pools [Allen and Day, 1935, p. 90; Werner and Brantley, 2003]. Notably, there can be wide geographic separation between thermal areas dominated by neutral Cl waters and those with acid sulfate terrain [Hurwitz *et al.*, 2007; Lowenstern and Hurwitz, 2008].

[3] White [1957] developed a model that linked the two disparate waters through boiling of subsurface neutral Cl water that produces an upflow of steam and gas that condenses in the near-surface to form “acid sulfate” areas of clay-rich, acid-altered terrain. He cited Steamboat Springs and Beowawe (both in Nevada) and Yellowstone as geothermal systems where neutral Cl and acid waters shared a linkage through boiling [see also Ellis and Mahon, 1977; Henley and Ellis, 1983; Hedenquist, 1991]. Though this model makes intuitive sense and is often used to describe and interpret hydrothermal activity around the world, there have been few assessments of the model in terms of heat and mass balance, water and gas chemistry, or isotopic variations of the emerging fluids (however, see Hedenquist [1991] for a discussion of Waiotapu, New Zealand). A major problem was that methods

to estimate steam and gas flux did not exist until the late 1990s [Werner *et al.*, 2000; Lewicki *et al.*, 2005; Chiodini *et al.*, 2005], so it was difficult to compare outputs of neutral waters to any potentially related steam and gas. Moreover, only a few studies at Yellowstone have included gas and water chemistry from nearby neutral and acid waters [e.g., Windman *et al.*, 2007, Hearn *et al.*, 1990].

[4] Heart Lake Geyser Basin (HLGB) (Figure 1) at the southern margin of the Yellowstone Caldera contains both acid and neutral Cl waters. The waters emerge at a variety of elevations along the Witch Creek drainage. At the highest elevations, acid-altered ground hosts a variety of acid springs and steaming ground. Neutral Cl waters discharge downslope and flow into Witch Creek, which feeds Heart Lake and eventually the Snake River. Though several workers have described this thermal area and the chemistry of its waters [Thompson *et al.*, 1975; Mazor and Thompson, 1982; Thompson and DeMonge, 1996; Ball *et al.*, 2001; Gemery-Hill *et al.*, 2007], until now there is no existing work that considers the geographic variability of water, gas, and isotope chemistry or that provides estimates of both the gas and thermal water flux.

[5] In 2009 we collected gas and water samples at the HLGB to provide a full suite of chemical and isotopic data. We also gauged stream discharge at various sites and measured the diffuse CO₂ flux at two areas of acid sulfate alteration. This work permits us to evaluate the heat and mass outputs and isotopic compositions of HLGB fluids, the subsurface temperature of this geothermal system, and the ultimate relationship of the Heart Lake area hydrothermal fluids with other hot spring areas at Yellowstone. The result is a thorough investigation of the evolution of thermal waters resulting from transport, boiling, and mixing. An additional novel aspect of this paper is that we are able to tie steam and gas output to near closed system boiling of the discharged thermal water. Nevertheless, we also find evidence for locally derived gas that is volumetrically minor but has a clear effect on the isotopic composition of C and He in emitted gases.

2. Background

2.1. Geologic and Hydrothermal Context

[6] The Heart Lake Geyser Basin sits at the intersection of the Yellowstone Caldera and active normal faults along the east side of the Red Mountains and Mount Sheridan (Figure 2). Springs at the

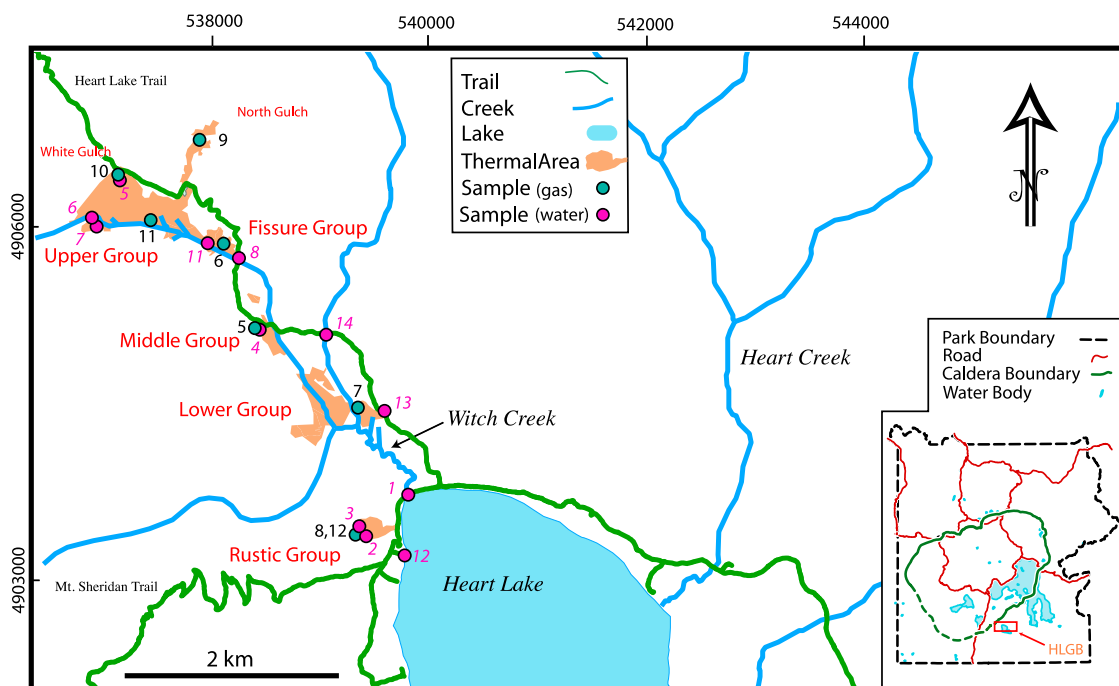


Figure 1. Sample localities for gas (green) and water (pink) samples in Tables 1 and 2. Thermal regions are shaded brown and are taken from Yellowstone National Park (Hydrogeothermal areas of Yellowstone National Park, Wyoming, Montana, Idaho, unpublished geodatabase, provided 2010). The inset shows the area of HLGB within Yellowstone National Park.

highest elevations at the HLGB issue along the Yellowstone Caldera ring fault (Caldera 3 in Figure 2) near intersections with the above mentioned faults. Other springs are found along Witch Creek, east of the range-bounding faults. The springs discharge outside the inferred limits of the postcaldera Aster Creek rhyolite flow and within the mapped area of glacial sediments [Christiansen, 2001]. It is possible that the most northwesterly springs discharge from the base of the Aster Creek flow. It is worth noting that the Red Mountain Caldera segment of the cycle I caldera (Huckleberry Ridge Tuff, erupted 2.1 Ma) cuts through the northern Red Mountains in the vicinity of Factory Hill (Figure 2).

[7] *Hayden* [1883] divided features in HLGB into five separate groups: four of which, the Upper, Fissure, Middle and Lower Groups, are located on and adjacent to Witch Creek, and the fifth, Rustic Group, is located 200 m west of Heart Lake (Figure 1). The Upper Group (Figure 3a) is at the highest elevation, farthest upstream along Witch Creek, and is the only group with acid waters [Thompson *et al.*, 1975; Ball *et al.*, 2001; Gemery-Hill *et al.*, 2007]. Neutral Cl waters emerge from all five groups. *Bryan* [2008] characterized

hydrothermal activity of the basin as “intense” but containing only small geysers with maximum discharge height around 20 m. Geyser activity has been noted at all the groups, though the Fissure Group (Figure 3b) is most active, and evidence of geysering in the Middle Group is limited only to a short time period in the 1980s [Bryan, 2008].

2.2. Previous Work

[8] The first detailed study of HLGB was performed by A. Peale in the 1870s [Hayden, 1883]. Their map defined the various thermal area groups shown in Figure 1, as well as the thermal barren known as White Gulch, adjacent to the Upper Group. *Allen and Day* [1935] added additional detail on temperatures and eruptive behavior of individual thermal features and estimated the total thermal water outflow for HLGB as 104 L s^{-1} . Later maps and descriptions of geysers at HLGB are given by *Bryan* [2008] (as well as earlier editions). An informal report by R. Papariello (The Heart Lake Geysers Basin, unpublished manuscript, 1988) contains photocopies of many early explorers’ accounts of the region, early U.S. Geological Survey reports, and unpublished data.

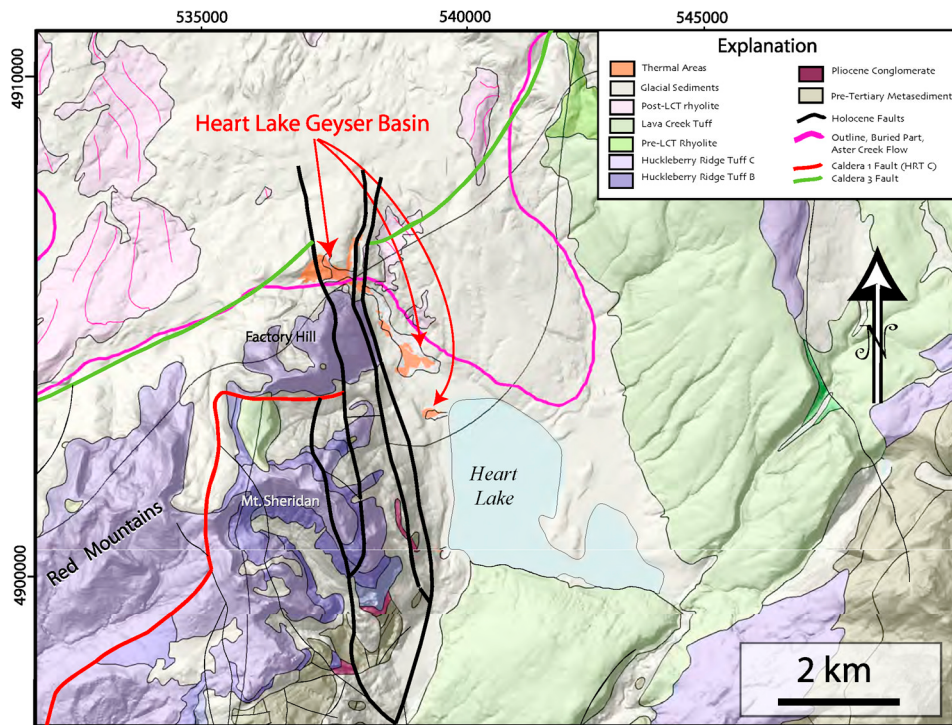


Figure 2. Geological framework of Heart Lake surroundings based on work by *Christiansen* [2001]. Heart Lake lies in a basin formed by normal, recently active faults to the east of the Red Mountains. The northwestmost springs emerge near the intersection of these faults and the Yellowstone Caldera boundary. LCT is the 640,000 year old Lava Creek Tuff. The Caldera 3 Fault was formed during eruption of the LCT, whereas the Caldera 1 Fault formed 2.1 Ma during eruption of the Huckleberry Ridge Tuff.

[9] Chemical analyses of waters from HLGB are listed in a variety of tabulations [*Thompson et al.*, 1975; *Thompson and DeMonge*, 1996; *Ball et al.*, 2001; *Gemery-Hill et al.*, 2007]. *Mazor and*

Thompson [1982] noted that neutral Cl waters from HLGB were geochemically similar to thermal springs from sinter-forming geothermal areas around Yellowstone, including Shoshone, Upper,

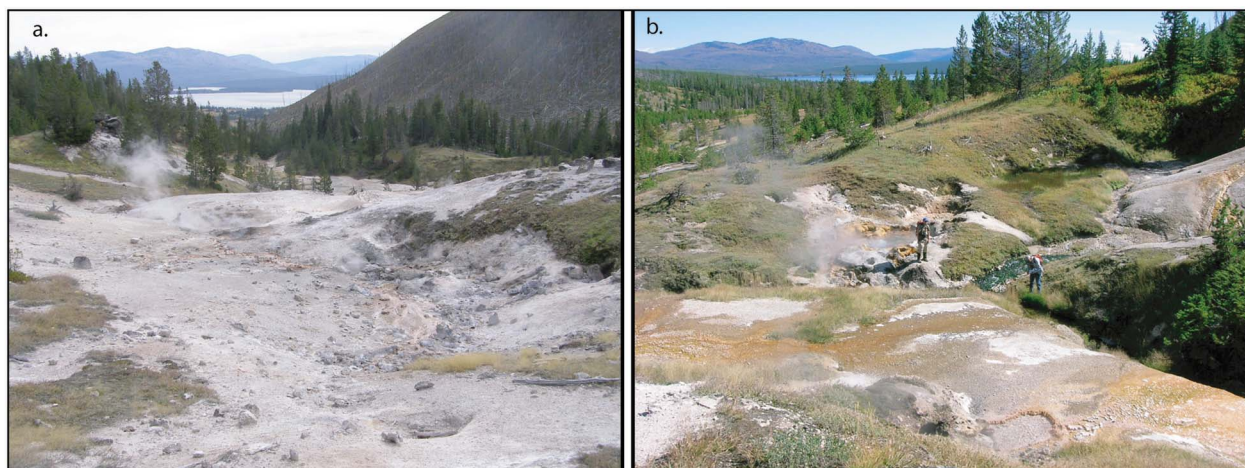


Figure 3. Photographs of varied thermal groups within the HLGB. (a) Steam-heated (acid sulfate) terrain of the Upper Group, where fumaroles and acid waters discharge from muddy, clay-dominated soils. Heart Lake is in background (4 km distant). (b) Fissure Group. Silica-saturated alkaline (neutral Cl) waters issue as springs and geysers to create landforms composed of silica sinter.

Midway, Lower and Norris geyser basins. They recognized, as had earlier workers, that Na and Cl are the dominant cation and anion, respectively. They concluded that a single relatively homogeneous parent fluid fed most of the hot spring systems in the west side of the park, including the above named basins [see also *Fournier et al.*, 1976, *Fournier*, 1989; *Rye and Truesdell*, 2007]. Furthermore, they noted that the HLGB (and other) waters exhibited tight positive correlations among dissolved Na, Cl, F, Li, B, and SiO₂ and that these waters could be related to a single deep parent fluid that was either diluted by mixing with groundwater or concentrated through boiling. High SO₄ concentrations relative to other areas at Yellowstone were believed to be due to interactions with sedimentary sulfate. Finally, *Mazor and Thompson* [1982] concluded that SiO₂ concentrations reliably reflected deep temperatures and mineral-buffered equilibria, whereas K concentrations were affected by near-surface reactions that made K-based geothermometers inaccurate. *Rye and Truesdell* [2007] noted that $\delta^{18}\text{O}\text{-Cl}$ relations at HLGB seemed consistent with some mixing of evaporated water from Heart Lake that had mixed into the deep parent fluid.

[10] Plots of gas compositions from the HLGB demonstrated that the gases were low in H₂ relative to crust-derived gases such as CH₄ [*Sheppard et al.*, 1992]. Isotopic analyses of noble gases revealed that HLGB samples contain more radiogenic (crustal) He than any other areas in or adjacent to the Yellowstone Caldera [*Kennedy et al.*, 1985].

3. Methods

3.1. Water Chemistry and Isotopes

[11] In September 2009 water samples were collected from hot springs, Witch Creek, Heart Lake and several tributaries to Witch Creek. At each sampling site we measured temperature and specific conductance with handheld meters and pH using a meter or indicator strips. Water samples were filtered through a 0.45 μm filter and collected in prerinsed plastic bottles. Samples for cation analyses were preserved by drop-wise addition of high-purity nitric acid to a pH less than 2. Raw water samples for stable isotopes were collected brim full in glass bottles. Alkalinity was measured in the field using sulfuric acid and a digital titrator. Chemical analyses were performed at the U.S. Geological Survey (USGS) in Menlo Park, California. Anion and cation concentrations were

determined with a Dionex ICS-2000 ion chromatograph and a ThermoFisher ICAP 6000 inductively coupled argon plasma optical emission spectrometer, respectively. Analytical uncertainties for all species are $\sim 5\%$. Stable isotope analyses were performed at USGS laboratories in Reston and Denver.

3.2. Water Discharge

[12] Discharge measurements were made by three methods depending in part on the characteristics and magnitude of the flow. Water discharge in Witch Creek and its upper tributaries was gauged by wading rod and pygmy meter using USGS protocol [*Schneider and Smoot*, 1976]. Small discharges from individual features were derived from the time required to fill a graduated plastic beaker positioned to capture the flow. Some intermediate-size discharges were determined from visual estimates of channel width and depth and velocity of small wood chips placed in the flow.

3.3. Gas Collection and Analyses

[13] Samples of gas plus steam were collected from fumaroles, bubbling pools, and boiling ground (“frying pans”). Steam and soluble gases were routed through a plastic funnel or a titanium tube and connected using Tygon tubing to a “Giggenbach” bottle, where steam condensed and CO₂ and H₂S dissolved in caustic (4N NaOH). The more inert gases (H₂, He, N₂, Ar, O₂, CH₄, and other hydrocarbons) were collected in the head space. At sites where noble gas isotope analyses were desired, a second sample was collected into a ~ 30 cm length of copper tubing. More information on collection methods is available from *Giggenbach and Goguel* [1989], *Fahlquist and Janik* [1992], and especially *Bergfeld et al.* [2011].

[14] Constituents of the head space in the Giggenbach bottles were determined by gas chromatography using a Varian CP-3800 equipped with dual thermal conductivity detectors and a flame ionization detector. Gases dissolved within the NaOH solution were either measured by manometry (CO₂), ion chromatography (Cl, F, and H₂S, the latter after oxidation to form SO₄), or gas-sensing electrode (NH₃) at the USGS volcano gas geochemistry laboratory in Menlo Park, California, according to procedures outlined by *Fahlquist and Janik* [1992], *Evans et al.* [2006], and *Bergfeld et al.* [2011]. Carbon dioxide was determined by injecting an aliquot of the caustic solution into an evacuated bottle, adding H₂O₂, and evolving the

gas using H_2SO_4 [Bergfeld *et al.*, 2011]. The evolved CO_2 was purified, quantified, and collected on a vacuum extraction line and was analyzed at the USGS stable isotope laboratory in Reston, Virginia. Helium and neon isotopes were determined on a sector mass spectrometer, and argon isotopes were determined on a quadrupole mass spectrometer at the USGS Noble Gas Laboratory in Denver, Colorado. In the text, R_c/R_a represents the $^3\text{He}/^4\text{He}$ ratio of the sample (corrected for any minor addition of air) divided by the same ratio in air.

[15] The gas chemistry in Table 2 is tabulated as the mole percent of steam-free gas. The percentage of gas is indicated by the %G value, which represents the mole percent of gas relative to the sum of steam plus gas (i.e., pure steam is 0 and pure gas is 100).

3.4. Diffuse CO_2 Gas Flux

[16] The diffuse CO_2 flux at HLGB was measured at 109 sites on 13 September 2009. Flux measurements were made using two West Systems flux meters equipped with LI-COR 820 infrared CO_2 analyzers using methods outlined by Lewicki *et al.* [2005]. The flux measurement grids were located in two discrete areas characterized by acid sulfate alteration, North Gulch (our informal name) and White Gulch, and were separated by about 700 m (Figure 1). Flux sites at North Gulch were located along a NNE-SSW trending valley, and the sites in White Gulch were situated across a hillslope.

[17] Individual measurement sites at each thermal area were based on a grid with points selected by pace and compass. Grid spacing in the North Gulch was between 10 and 15 m, and at White Gulch spacing was about 20 m but was more variable due to topography. Our coverage of North Gulch included 63 sites over an area $\sim 42,700 \text{ m}^2$. Coverage of White Gulch was irregular and included 41 sites across $\sim 48,000 \text{ m}^2$. Calculations for total diffuse emissions are based on the mean flux for each grid multiplied by the grid area and are reported as metric tons of CO_2 per day (t d^{-1}). Gas samples were collected from a fumarole within each grid.

4. Results

4.1. Water Chemistry

[18] Acid and neutral Cl waters emerge at temperatures up to the boiling point of H_2O ($\sim 93^\circ\text{C}$ at the local elevation of $\sim 2300 \text{ m}$). We observed and sampled muddy, acid sulfate features only in the Upper Group, consistent with previous work.

[19] As reported previously [Thompson *et al.*, 1975; Thompson and DeMonge, 1996; Ball *et al.*, 2001; Gemery-Hill *et al.*, 2007], nonacid waters, with temperatures from ambient up to boiling, have elevated Na, Cl, and SiO_2 (Table 1). Field- and laboratory-measured pH values range from ~ 8 to nearly 10; that is, these waters are primarily alkaline, but we retain the terminology “neutral Cl” for consistency with previous studies. Plotted on a $\text{HCO}_3\text{-SO}_4\text{-Cl}$ ternary (Figure 4, bottom) they overlap with the compositions of cold waters from Heart Lake and form a linear trend between boiling neutral Cl waters (circled in Figure 4) and dilute $\text{HCO}_3\text{-rich}$ waters. Snake River waters are also shown in Figure 4 and were sampled at a stream gage located 35 km downstream from Heart Lake near the park’s south entrance. Higher SO_4 concentrations in the Snake River waters likely reflect input from Paleozoic and Mesozoic metasediments present to the south of the Yellowstone Caldera. In contrast, acid waters from the HLGB (e.g., W5) are enriched in SO_4 but contain minimal Cl (Table 1).

[20] On a cation ternary diagram (Figure 4 (top), red ternary), neutral Cl waters lie along the Na-K sidebar, though at more Na-rich compositions than some other neutral Cl waters from Yellowstone. Such Na/K ratios reflect water-rock equilibration at geothermal temperatures ($\sim 200^\circ\text{C}$) with feldspar-bearing rocks such as Yellowstone rhyolites [Ellis and Mahon, 1977]. In contrast, acid water from the Upper Group plots in the K-rich apex, consistent with direct dissolution of Yellowstone rhyolites [Hedenquist *et al.*, 1994]. Heart Lake itself plots in between the neutral Cl waters and Mg- and Ca-rich cold, dilute waters as typified by samples from the Snake River.

[21] The maximum Cl concentration in the sampled neutral Cl waters is 350 mg L^{-1} , just below the maximum of 370 mg L^{-1} found by earlier workers (Figures 5a and 5b). Our data together with that of earlier workers demonstrate strong correlations between Cl and solutes such as Na, Li, F, and SO_4 ($R^2 = 0.96, 0.94, 0.89,$ and 0.83 , respectively) with linear trends passing close to the origin. SiO_2 concentrations also correlate with Cl ($R^2 = 0.89$), and maximum measured concentrations from HLGB are $\sim 400 \text{ mg L}^{-1}$ [Thompson *et al.*, 1975], somewhat higher than the 369 mg L^{-1} maximum value we found (Table 1). In detail, these trends do not pass exactly through the origin because the cold dilute waters would contain some solutes [Hurwitz *et al.*, 2010].

Table 1. Chemistry, Isotopic Composition and Characteristics of Water Samples From HLG^B

Sample	Short Name														
	W1	W2	W3	W4	W5	W6	W7	W8	W11	W12	W13	W14	W14	W14	
Location	YNP09- HL01 Witch Creek at Heart Lake	YNP09- HL02 Columbia Spring outflow	YNP09- HL03 Rustic Geyser outflow	YNP09- HL04 Hot Spring at G5	YNP09- HL05 Acid Outflow at G10	YNP09- HL06 North fork Witch Creek	YNP09- HL07 South fork Witch Creek	YNP09- HL08 Witch Creek Upper Bridge	YNP09- HL11 Fissure Spring	YNP09- HL12 Heart L.	YNP09- HL13 Witch Creek Tributary1	YNP09- HL14 Witch Creek Tributary2	YNP09- HL14 Witch Creek Tributary2	YNP09- HL14 Witch Creek Tributary2	YNP09- HL14 Witch Creek Tributary2
Group	-	Rustic	Rustic	Middle	Upper	-	-	-	Fissure	-	-	-	-	-	-
Date 2009	11 Sep	11 Sep	11 Sep	12 Sep	12 Sep	12 Sep	12 Sep	13 Sep	13 Sep	13 Sep	14 Sep	14 Sep	14 Sep	14 Sep	14 Sep
Temp (°C)	26.4	85.8	41	89.6	20.1	16	10.8	45.4	84.3	16.4	27.4	18.9	18.9	18.9	18.9
pH (F)	8.80	7.72	8.79	7.62	2.80	7.26	7.14	9.03	9.5 (s)	6.5 (s)	7.5 (s)	5.5 (s)	5.5 (s)	5.5 (s)	5.5 (s)
pH (L)	8.91	8.02	9.36	7.95	n.m.	7.30	7.26	9.40	9.91	9.06	7.76	7.85	7.85	7.85	7.85
Conductance (μ S/cm)	525	1822	2100	1355	n.m.	74	33.8	638	2030	230	478	196	196	196	196
Discharge (L/s)	223	7.1	n.m.	0.096	0.018	14	7.0	74	n.m.	n.m.	2.8	17	17	17	17
Method ^a	G	V	n.m.	B	B	G	G	G	n.m.	n.m.	V	V	V	V	V
Easting (m)	539799	539398	539336	538455	537292	537080	537018	538309	538033	539743	539582	539030	539030	539030	539030
Northing (m)	4903630	4903295	4903347	4905116	4906347	4906039	4905916	4905702	4905799	4903185	4904360	4905039	4905039	4905039	4905039
Elevation (m)	2268	2295	2289	2315	2449	2424	2430	2293	n.m.	2273	2310	2297	2297	2297	2297
δ D per mill	-136	-140	-136	-144	-119	-136	-136	-138	-140	-120	-141	-138	-138	-138	-138
δ^{18} O per mill	-17.6	-15.9	-15.0	-17.9	-13.5	-18.3	-18.3	-17.8	-16.7	-14.9	-18.3	-18.1	-18.1	-18.1	-18.1
Alk (as HCO ₃)	99	320	341	280	0	47	20	116	299	51	137	65	65	65	65
Al	0.03	0.34	0.26	<0.005	1.62	0.01	<0.005	0.06	0.27	0.01	<0.005	0.01	0.01	0.01	0.01
As	0.29	1.23	1.34	0.97	0.003	0.003	0.001	0.46	1.34	0.07	0.01	0.003	0.003	0.003	0.003
B	0.95	3.89	4.23	2.85	0.07	<0.01	<0.01	1.29	4.47	0.31	0.63	0.18	0.18	0.18	0.18
Ba	0.01	<0.005	<0.005	0.02	0.09	0.01	0.02	0.01	<0.005	0.01	0.01	0.01	0.01	0.01	0.01
Br	0.196	0.876	0.948	0.652	0.002	<0.002	<0.002	0.282	1.060	0.051	0.134	0.033	0.033	0.033	0.033
Ca	3.7	0.89	0.99	8.3	1.9	7.6	3.1	2.6	0.95	4.1	16.0	6.6	6.6	6.6	6.6
Cd	<0.002	0.01	0.01	<0.005	<0.001	<0.001	<0.001	0.002	0.01	<0.001	<0.002	<0.001	<0.001	<0.001	<0.001
Cl	72.4	300	324	222	0.36	0.38	0.25	96.7	350	24.6	49.8	13.2	13.2	13.2	13.2
Co	<0.002	<0.005	<0.005	<0.005	<0.001	<0.001	<0.001	<0.002	<0.005	<0.001	<0.002	<0.001	<0.001	<0.001	<0.001
Cr	<0.01	<0.025	<0.025	<0.025	<0.005	<0.005	<0.005	<0.01	<0.025	<0.005	<0.01	<0.005	<0.005	<0.005	<0.005
Cu	<0.002	<0.005	<0.005	<0.005	<0.001	<0.001	<0.001	<0.002	<0.005	<0.001	<0.002	<0.001	<0.001	<0.001	<0.001
F	7.4	25.4	27.4	16.0	0.14	0.18	0.06	8.8	30.7	2.7	7.7	6.2	6.2	6.2	6.2
Fe	0.041	<0.005	<0.005	0.050	2.27	0.069	0.026	0.039	<0.005	0.022	0.011	0.050	0.050	0.050	0.050
K	7.6	17.2	12.6	10.7	13.9	2.5	1.3	8.8	29.3	3.4	8.6	4.1	4.1	4.1	4.1
Li	1.2	6.0	6.2	3.5	<0.01	<0.01	<0.01	1.6	5.8	0.36	0.67	0.17	0.17	0.17	0.17
Mg	0.464	<0.005	<0.005	0.208	0.306	2.09	0.874	0.474	<0.005	0.757	1.96	0.716	0.716	0.716	0.716
Mn	0.004	<0.005	<0.005	0.059	0.063	0.005	0.011	0.003	<0.005	0.002	<0.002	0.006	0.006	0.006	0.006
Mo	0.022	0.093	0.104	0.063	<0.001	<0.001	<0.001	0.028	0.094	0.007	0.016	0.008	0.008	0.008	0.008
Na	104	413	446	301	4.5	4.3	2.3	12.5	427	36	78	32	32	32	32
Ni	<0.002	<0.005	<0.005	<0.005	<0.001	<0.001	<0.001	<0.002	<0.005	<0.001	<0.002	<0.001	<0.001	<0.001	<0.001
PO ₄	<0.01	<0.04	0.04	<0.04	<0.01	0.01	<0.01	0.01	0.04	<0.01	<0.01	<0.01	<0.01	<0.01	<0.01

Table 1. (continued)

	Short Name													
	W1	W2	W3	W4	W5	W6	W7	W8	W11	W12	W13	W14		
Rb	0.0570	0.2255	0.1467	0.1087	0.0559	<0.01	<0.01	0.0928	0.3783	0.0166	0.0358	0.0208		
Se	<0.002	<0.005	<0.005	<0.005	0.001	<0.001	<0.001	<0.002	<0.005	<0.001	<0.002	<0.001		
SiO ₂	104	300	369	205	251	47.4	20.7	125	332	23.8	102	88.9		
SO ₄	41.3	153	164	113	149	2.9	0.85	56	180	13.1	27	10.3		
Sr	0.0171	0.0266	<0.005	0.0688	0.0130	0.0277	0.0166	0.0158	0.0136	0.0180	0.0314	0.0169		
Zn	0.0021	0.0157	<0.005	<0.005	0.0330	<0.001	<0.001	<0.002	<0.005	<0.001	<0.002	0.0012		
TDS	439	1540	1657	1163	425	115	50	529	1581	157	428	227		
Cation sum	5.1	19.3	20.7	14.3	2.6	0.8	0.4	6.1	20.2	2.0	4.6	1.9		
Anion sum	4.9	18.3	19.6	14.1	3.1	0.9	0.4	6.3	20.2	1.9	4.6	2.0		
Balance	3.7%	5.7%	5.1%	1.4%	-18.3%	-5.9%	1.6%	-3.1%	0.2%	0.4%	0.7%	-3.0%		

^aWater discharge was either gauged (G); determined by filling a plastic beaker (B); or visually estimated (V); n.m., not measured; all units in mg L⁻¹ unless otherwise noted; pH(F) = pH measured in the field using a meter or indicator paper; pH(L) = pH measured in the laboratory using a meter. Detection limits vary according to analytical conditions. Charge imbalance for W5 is likely due to small pH error.

4.2. The δD and $\delta^{18}\text{O}$ Values for HLGB Water

[22] The four high-temperature neutral Cl waters we sampled all have δD values between -144‰ and -136‰ (Figure 6), consistent with other neutral Cl fluids from Yellowstone [Rye and Truesdell, 2007; Bergfeld et al., 2011]. The waters plot significantly to the right of the global meteoric water line, as is common for hydrothermal waters throughout the world that have exchanged oxygen with local wall rocks [Truesdell and Hulston, 1980]. Sample W4, the most dilute of the neutral Cl hot spring waters, also has the lightest δD and $\delta^{18}\text{O}$ values; the two samples from the Rustic Group have the heaviest values (Figure 6).

[23] Acid waters from HLGB are heavier (more positive) in both δD and $\delta^{18}\text{O}$ than the neutral Cl waters with δD extending up to -119‰ , as is typical for evaporated surface waters [Nordstrom et al., 2005, 2009]. As expected, steam condensates from two fumaroles are significantly lighter and plot on the left side of the global meteoric water line. The lightest of those two samples has a δD value of -167‰ (Table 2). The isotopic composition of waters from Witch Creek and its local tributaries plot along the global meteoric water line, or between it and high-temperature neutral Cl waters.

4.3. Water and Solute Flux

[24] The outflow from Witch Creek at its entrance to Heart Lake was measured at 223 L s^{-1} (Table 3). The Cl concentration of Witch Creek at that point was 72.4 mg L^{-1} , about 20% of that found in the most concentrated neutral Cl waters. Witch Creek, at its confluence with Heart Lake, should consist of a mixture of concentrated and diluted thermal waters, nonthermal water from cold springs and assorted tributaries, and minor acid waters from the Upper Group. As such, it is difficult to compare our discharge values with those of Allen and Day [1935], who directly measured discharge of thermal waters and estimated 3.67 cfs (104 L s^{-1}). If the mean HLGB thermal water (including subboiling waters) had 160 mg L^{-1} Cl, then Witch Creek would consist of 45% thermal water or about 105 L s^{-1} of thermal water, similar to the value measured by Allen and Day [1935]. However, because we and most researchers have sampled only the hottest fluids, it is not straightforward to estimate the mean HLGB thermal water; we conclude simply that our

Table 2. Chemistry and Isotopic Composition of HLGB Gas Samples^a

	Short Name							
	G5	G6	G7	G8	G9	G10	G11	G12
Sample	YL09-05	YL09-06	YL09-07B	YL09-08	YL09-09	YL09-10	YL09-11	YL09-12
Group	Middle	Fissure	Lower	Rustic	Upper/North	Upper/White	Upper	Rustic
Type	Pool	Fum	Pool	Fum	Fum	Fum	Fry	Fum
Easting	538455	538183	539343	539330	537947	537259	537568	539330
Northing	4905116	4905810	4904383	4903255	4906671	4906392	4906016	4903255
Temp (°C)	89.9	92.9	84	93.0	92.9	92.7	92.0	93.4
%G	3.91	0.18	62.3	0.06	0.30	0.38	0.17	0.06
CO ₂	96.8	95.5	64.8	83.5	93.3	93.7	93.5	86.1
H ₂ S	0.045	0.755	0.021	0.667	0.608	0.641	1.155	0.77
NH ₃	0.005	0.072	0.000	0.368	0.030	0.000	0.000	0.217
He	0.005	0.014	0.018	0.067	0.020	0.013	0.014	0.0426
H ₂	0.002	0.100	0.005	0.023	0.076	0.059	0.173	0.031
Ar	0.075	0.075	0.423	0.311	0.101	0.104	0.093	0.2332
O ₂	0.135	0.009	6.675	0.039	bdl	0.002	0.005	bdl
N ₂	2.29	2.20	27.05	10.49	3.74	3.65	3.44	8.74
CH ₄	0.629	1.239	1.011	4.545	2.077	1.867	1.571	3.8765
C ₂ H ₆	0.00218	0.00517	0.00416	0.01538	0.00890	0.00884	0.00759	0.01408
C ₃ H ₈	0.00038	0.00131	n.m.	0.00525	0.00352	0.00347	0.00275	0.00489
C ₄ H ₁₀	0.00009	0.00034	n.m.	0.00156	0.00104	0.00100	0.00068	0.00137
N ₂ /Ar	30.4	29.4	64.0	33.7	37.2	35.2	36.9	37.5
H ₂ -Ar Temp	63	184	43	96	166	158	194	114
Δ ¹³ C Temp	149	137	-	-	169	195	-	-
Rc/Ra	1.20	1.14	n.m.	1.09	1.81	2.67	2.91	n.m.
± Rc/Ra	0.01	0.01	-	0.01	0.01	0.01	0.01	-
δ ¹³ C CO ₂	-4.7	-3.4	-4.4	n.m.	-3.0	-2.0	n.m.	n.m.
δ ¹³ C CH ₄	-44.2	-44.1	n.m.	-43.2	-40.5	-36.8	-36.5	-43.2
δD _{steam}	n.m.	n.m.	n.m.	n.m.	n.m.	-166.6	-155.4	n.m.
δ ¹⁸ O _{steam}	n.m.	n.m.	n.m.	n.m.	n.m.	-23.9	-21.8	n.m.

^aGas abundances in mol %; %G is mol % gas relative to gas + steam. H₂-Ar Temp calculated with equations from *Giggenbach and Goguel* [1989]; Δ¹³C temperature is from equations of *Horita* [2001]; δ¹³C, δD and δ¹⁸O are in per mill relative to the relevant standard (see text). Sample G5 is gas sampled from the same pool as W4; n.m., not measured; bdl, below detection limit, which is 0.0001 mol% for O₂. Dash means not calculable.

estimate is within ~25% of Allen and Day's estimate.

[25] In all, Witch Creek discharged about 16.2 g s⁻¹ of Cl and 9.2 g s⁻¹ of SO₄ to Heart Lake in September 2009. Comparing the Witch Creek solute flux just below the Fissure Group (W8) with that at the Heart Lake Confluence (W1), it is clear that ~44% of these anions were added by the Upper and Fissure Group waters, with the remainder coming from the Middle and Lower Groups. The two Witch Creek tributaries sampled above the Upper Group, W6 and W7, were dilute. Another 2.1 g s⁻¹ of Cl and 1.1 g s⁻¹ of SO₄ discharged from the Rustic Group directly into Heart Lake. In total, 18.3 g s⁻¹ of Cl and 10.3 g s⁻¹ of SO₄ were discharged from the HLGB (Table 3).

[26] Averaging our data plus that available in the literature (references cited for Figure 5) reveals that the mean, near-boiling neutral Cl water at HLGB contains ~299 ± 53 mg L⁻¹ Cl. The emission of

18.3 g s⁻¹ thus converts to 5.3 ± 1 t d⁻¹ (61 ± 11 L s⁻¹) of boiling, neutral Cl thermal water that emerged to the surface and flowed into the lake during our sampling in September 2009. From a comparison with results from *Hurwitz et al.* [2007] we expect that value would vary less than 20% from season to season and year to year.

4.4. Diffuse CO₂ Flux

[27] The average CO₂ flux at North Gulch was 54 g m⁻² d⁻¹, compared with the lower average of 29 g m⁻² d⁻¹ at White Gulch. The measured fluxes are much lower than in areas that contain only acid sulfate waters such as Hot Spring Basin (320 ± 74 g m⁻² d⁻¹ [*Werner et al.*, 2008]) and Mud Volcano (540 ± 96 g m⁻² d⁻¹ [*Werner and Brantley*, 2003]) and are far more similar to the 27 g m⁻² d⁻¹ found by *Werner and Brantley* [2003] at the Upper Geyser Basin, a thermal area

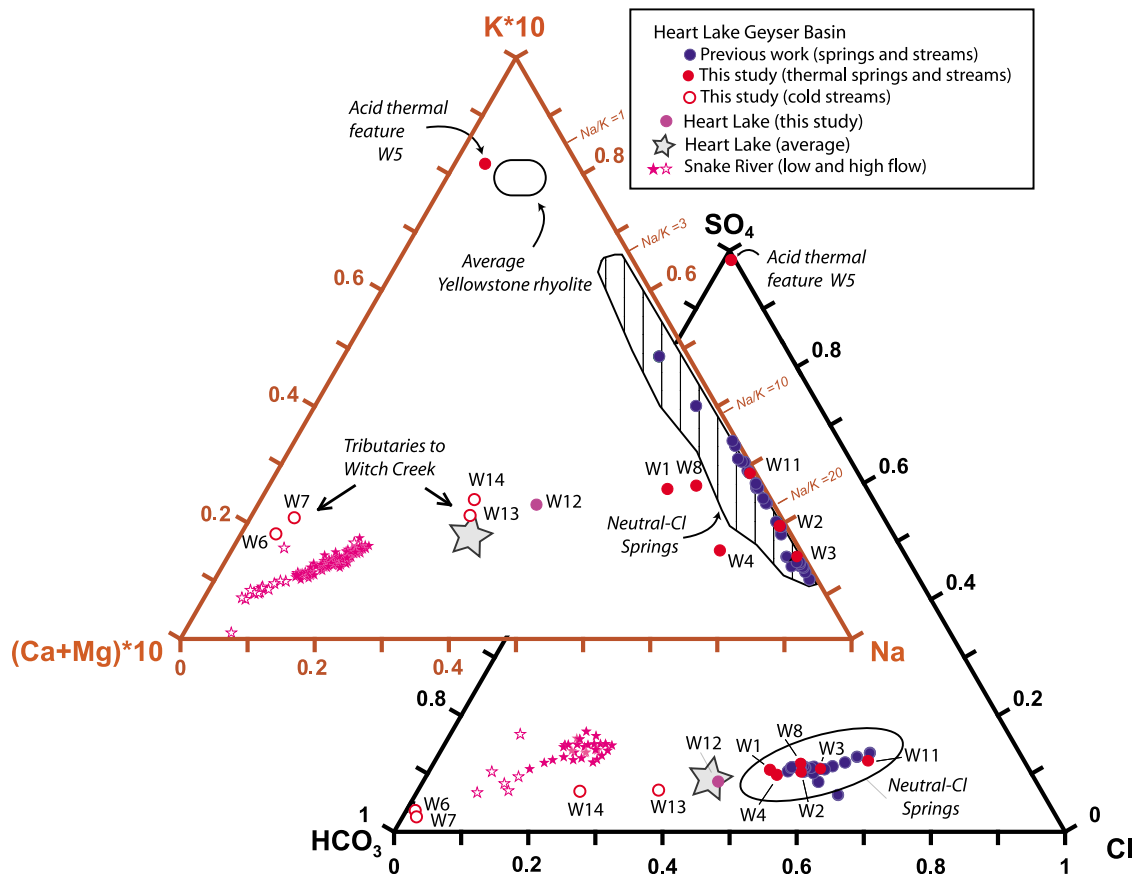


Figure 4. Molar composition plots of HLGB waters compared with nearby stream and lake waters. (top) Red axes, ternary, cation proportions demonstrate that HLGB thermal waters (red and blue dots) are Na-rich but that Witch Creek tributaries trend toward low-temperature (Ca+Mg-rich) waters (red outlined dots). Heart Lake waters (star and purple dot) are intermediate between HLGB waters and local cold waters, including those of the Snake River (pink stars). The highest-temperature waters are Mg- and Ca-poor and are similar to other Yellowstone neutral Cl waters (lined regions from *Hurwitz et al.* [2010]). The analyzed acid water is K-rich and plots close to the composition of average Yellowstone rhyolite [*Christiansen, 2001*]. Na/K mass ratios on the Na-K*10 axis allow easy comparison with values in Table 1. (bottom) Black axes, ternary, anion ratios demonstrate that Snake River waters have relatively lower Cl and higher SO₄ than the outflow from Heart Lake. The acidic sample, W5, plots near the SO₄ apex. Water from Heart Lake plots intermediate between the HLGB waters and cold tributary waters. Samples from previous work are from *Thompson et al.* [1975], *Thompson and DeMonge* [1996], and *Gemery-Hill et al.* [2007]. Heart Lake data are from *Theriot et al.* [1997].

that lacks acid sulfate waters and discharges only neutral to alkaline waters like those at HLGB.

[28] Our estimates of the total diffuse flux across the measured areas (42,700 m² and 48,000 m²) indicate that about 2.3 t d⁻¹ and 1.4 t d⁻¹ of CO₂ is discharged at North Gulch and White Gulch, respectively. *Werner et al.* [2000] defined the natural background flux as 19 g m⁻² d⁻¹ for Yellowstone. Using this value as the baseline CO₂ discharged at HLGB, we find that about 63% of the sites at North Gulch and 35% of those at White Gulch had CO₂ flux above background. Simple subtraction of the natural background flux from the

total discharge indicates anomalous CO₂ output from the two areas of ~2.0 t d⁻¹. If the average flux were extended to the entire Upper and Fissure Group areas (4.6 × 10⁵ m²), regions with observed potential for diffuse soil flux, as much as 10.4 t d⁻¹ (120 g s⁻¹) could plausibly be derived from HLGB. Such an estimate would be a maximum possible diffuse CO₂ flux for HLGB (Table 3).

4.5. Gas Chemistry

[29] Fumarolic samples from the HLGB were notably rich in steam, as is the case in other areas where neutral Cl waters emerge [*Bergfeld et al.*,

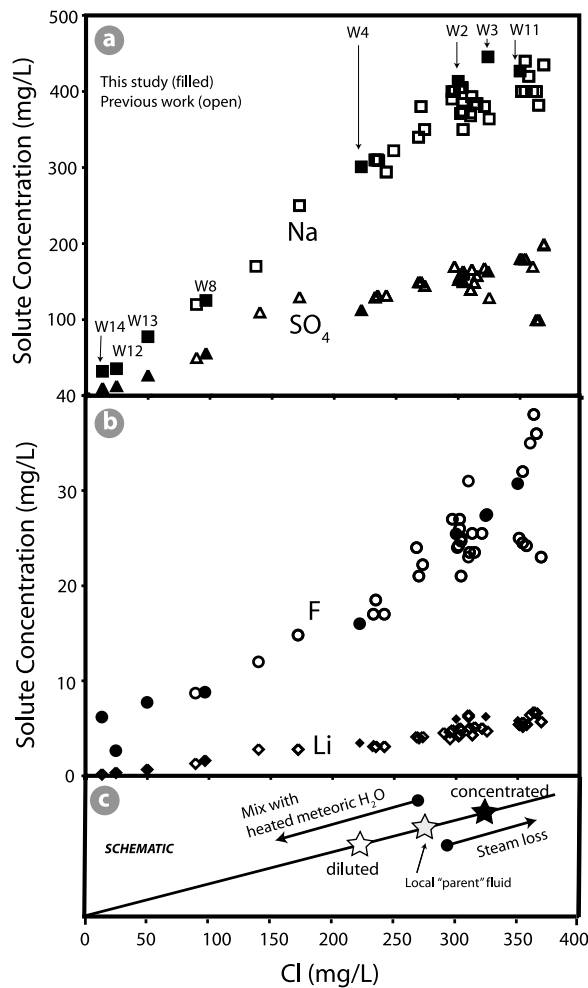


Figure 5. Plots showing Cl versus various solutes from nonacid waters of HLGB, including data from this study and previous work [Thompson *et al.*, 1975; Thompson and DeMonge, 1996; Gemery-Hill *et al.*, 2007]. (a) Na and SO₄ versus Cl demonstrate clear correlations of the three solutes. (b) Similar relations exist with F and Li. (c) Schematic plot indicates that HLGB neutral Cl waters appear to form a trend made up of an initial parent water (gray star) that is either variably diluted by solute-poor groundwater (white star, similar to W4) or concentrated through boiling (black star, similar to W3).

2011]. All of the fumarolic samples had %G values below 0.2, meaning that > 99.8 mol % of the discharge was steam (Figure 7 and Table 2). Of the remaining “noncondensable” gas contents (i.e., neglecting H₂O), CO₂ was dominant, but N₂, Ar, and CH₄ were notably high compared with other Yellowstone fumaroles (Table 2). Also evident was the relatively low H₂ concentrations. H₂ abundance relative to Ar can be used as an indicator of geothermal temperatures when gases are derived directly from boiling of geothermal water that

originated solely as meteoric water [Giggenbach, 1980; Giggenbach and Goguel, 1989; Chiodini and Marini, 1998]. As temperature increases, so does the equilibrium abundance of H₂ in steam. By using the H₂/Ar geothermometer of Giggenbach and Goguel [1989], we calculate temperatures up to 194°C (Table 2), with the highest temperatures at the uphill, western side of the HLG. Introduction of additional meteoric Ar during subsurface flow (Figures 7 and 8) clearly adds Ar and other shallowly derived gases that lower the calculated H₂/Ar temperature.

[30] Unlike many other regions of Yellowstone, gases from HLG do not plot on a simple trend of a well-mixed deep gas (represented by a constrained He/CH₄ ratio) with air-saturated meteoric water

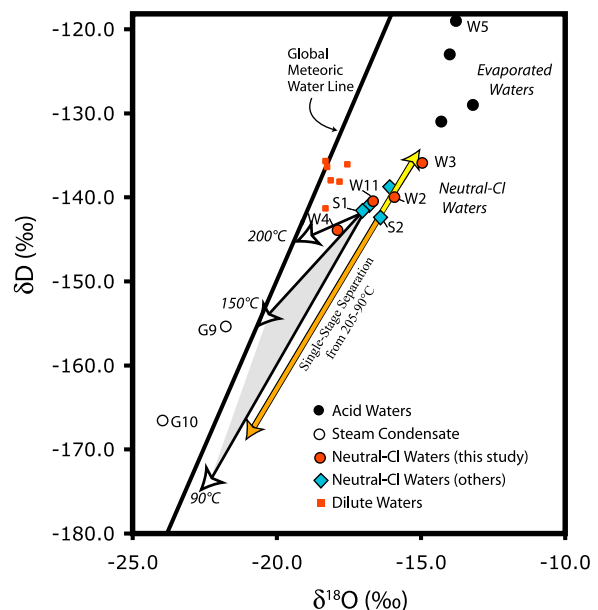


Figure 6. Plot of δD versus $\delta^{18}O$ for various waters from HLGB. Neutral Cl waters plot to the right of the global meteoric water line ($\delta D = 8 \cdot \delta^{18}O + 10$). Acid waters are shifted to heavier values (up and to the right), consistent with their being residual after evaporation under near-surface conditions. Steam condensates are significantly lighter (down and to the left), consistent with their origin as vapor produced through near-surface or possibly deeper boiling of the neutral Cl waters. Black vectors represent instantaneous boiling at relevant temperatures calculated with equations from Horita and Wesolowski [1994]. The yellow arrowhead points to the composition of residual liquid after boiling and single-stage steam separation of sample S2 from 205°C to 90°C. The separated steam would plot at the end of the orange arrow. Other data are from Gemery-Hill *et al.* [2007] and Ball *et al.* [2001].

Table 3. Measurements and Estimates of Solute Flux, Heat Flux, and Fluid Chemistry at HLGB

Item	Subject	Emissions	Uncertainty	Section	Assumptions
<i>Mass Flux</i>					
A	Water outflow Witch Creek	223 L s ⁻¹	±11	4.3	Measured
B	Cl flux	18.3 g s ⁻¹	±1.0	4.3	Measured
C	SO ₄ flux	10.3 g s ⁻¹	±1.0	4.3	Measured
D	Calculated discharge neutral Cl water	61.1 L s ⁻¹	±11.3	4.3	Item "B" with mean Cl concentration of 299 mg L ⁻¹
E	Calculated steam flux from HLGB	1.66 x 10 ⁴ g s ⁻²	±3.6 × 10 ³	5.5	Steam produced during boiling for D (21%)
F	Calculated input of thermal water to HLGB	77.7 L s ⁻¹	±15.5	5.5	D + liquid equivalent of E
G	CO ₂ flux at White Gulch	29 g m ⁻² d ⁻¹	±5	4.4	Measured
H	CO ₂ flux at North Gulch	54 g m ⁻² d ⁻¹	±8	4.4	Measured
I	Upper Group measured net CO ₂ discharge	22.9 g s ⁻¹	±8.0	4.4	background of 19 g m ⁻² d ⁻¹ and area of 90,800 m ²
J	Upper and Fissure Groups max CO ₂ discharge	120 g s ⁻¹	±48	4.4	same as I but assumes area of 460,000 m ²
K	Calculated CO ₂ discharge from CO ₂ /H ₂ O of fumaroles	72 g s ⁻¹	±17	5.6	mass CO ₂ /steam= 0.0043, E
<i>Heat Flux</i>					
L	Total HLGB heat discharge	68.0 MW	±13.8	5.7	F at 205°C
M	Heat discharge as steam	44.2 MW	±9.7	5.7	E at 93°C
N	Heat discharge as water	23.8 MW	±5.2	5.7	D at 93°C
<i>Concentrations and Pressures</i>					
O	Cl concentration Witch Creek	72.4 mg L ⁻¹	±3.6	4.3	Measured
P	Bulk CO ₂ in calculated HLGB parent water	21 mmol L ⁻¹	±7	5.6	F and K
Q	CO ₂ pressure in calculated HLGB parent water	230 kPa	±70	5.6	P at 205°C

(see Figure 8 of *Bergfeld et al.* [2011], reproduced as Figure S1 in the auxiliary material).¹ Instead, fumarolic gases from HLGB have a relatively constant ratio of deep to shallow gas, with varying He/CH₄.

[31] H₂S concentrations did not vary appreciably within the HLGB, as all concentrations in fumaroles were between 0.61% and 0.75%. Similarly, there are no obvious trends in H₂S ratios with less soluble gases (e.g., He), from the upper acid sulfate areas compared with the Rustic Group.

4.6. Gas Isotopes

[32] Compared with many areas at Yellowstone, the isotopic composition of CO₂ in HLGB gases exhibits greater than normal variation, with the δ¹³C content of CO₂ ranging from -2.0‰ to -4.7‰ VPDB (Table 2). The average δ¹³C value of 110 samples of Yellowstone CO₂ is -3.4‰ [*Bergfeld et al.*, 2011], somewhat lighter than that measured at the two acid sulfate fumaroles in the Upper Group at HLGB. As shown in Figure 8, δ¹³C values of CO₂ and CH₄ generally decrease to the

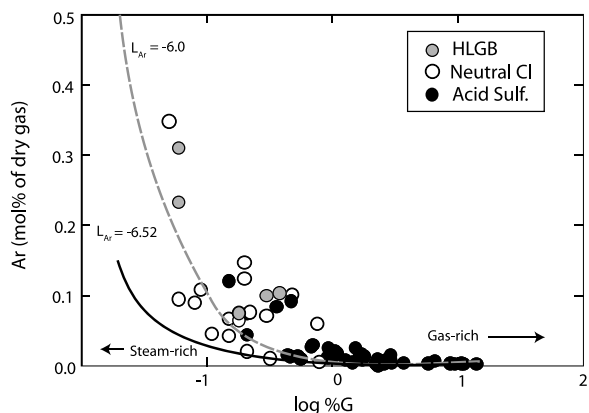


Figure 7. Mol% Ar versus log %G (i.e., 10% gas is log %G = 1) for Yellowstone fumaroles. Gas-rich samples have relatively low levels of Ar compared with steam-rich samples that are dominated by boiling of air-saturated meteoric water. Data are from *Bergfeld et al.* [2011]. Fumaroles from neutral Cl areas include Upper, Lower, Norris, and Gibbon geyser basins. The black curve represents a binary mixture of samples with %G = 20 and %G = 0.02 with all Ar assumed to be derived from boiled meteoric water (i.e., L_{Ar} or $\log(Ar/H_2O) = -6.52$ [*Giggenbach and Goguel*, 1989]). The gray dashed line incorporates additional (crustal) Ar so that $L_{Ar} = -6.00$.

¹Auxiliary materials are available in the HTML. doi:10.1029/2011GC003835.

southeast, in contrast to the ratio of CH_4 to C_2H_6 (C_1/C_2). The sample from the bubbling pool in the Middle Group had the lowest ^{13}C value for CO_2 and CH_4 . Carbon isotope analyses were not obtained for the Rustic Group due to the low CO_2 content of the gas. All samples plot at C_1/C_2 ratios and carbon isotope values consistent with abiogenic methane and ethane mostly created by reaction of H-C-O gas species at geothermal temperatures [Pohlman et al., 2009]. The fractionation of ^{13}C between CH_4 and CO_2 can be used as a geothermometer in situations where shallow mixing of gas sources is minimized [Horita, 2001, equation 6]. The maximum temperature for HLGB estimated by this technique is 195°C (Table 2). Lower apparent temperatures are calculated for samples collected farther down Witch Creek.

[33] A southeasterly (downhill) decline in the He isotope ratio mirrors the trend in $\delta^{13}\text{C}$ CH_4 (Figure 8). Helium in HLGB gases has some of the lowest Rc/Ra values within the Yellowstone Caldera [Kennedy et al., 1985; Bergfeld et al., 2011]. Across all of Yellowstone, Rc/Ra decreases with increasing He concentration (Figure 9) and is well illustrated at HLGB where Rc/Ra drops from 2.67 at White Gulch (130 ppm He) down to 1.09 in the He-rich (670 ppm He) sample from the Rustic Group. The decreased Rc/Ra ratio is clearly not due to contribution of air or air-saturated meteoric water, as the He/Ar of the Rustic Group sample

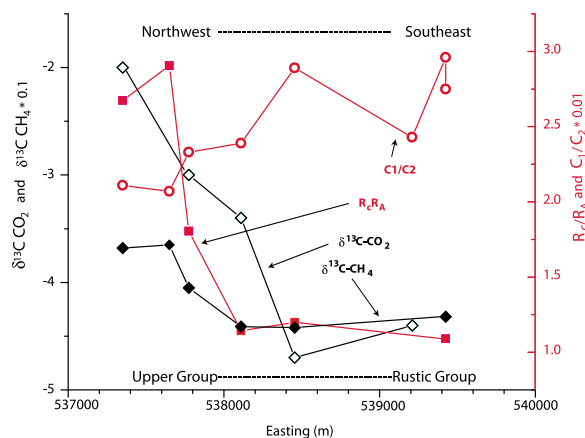


Figure 8. The $\delta^{13}\text{C}$ CO_2 and $0.1 \times \delta^{13}\text{C}$ CH_4 (symbols outlined in black and left axis) and $\text{R}_\text{C}/\text{R}_\text{A}$ and $0.01 \times \text{C}_1/\text{C}_2$ (symbols outlined in red and right axis) versus easting in meters. Toward the southeast, fumarole and frying pan gases have lower values of $\delta^{13}\text{C}$ CO_2 , $\delta^{13}\text{C}$ CH_4 , and $\text{R}_\text{C}/\text{R}_\text{A}$, apparently due to addition of crustal and biogenic components, the latter seemingly evident through increased C_1/C_2 .

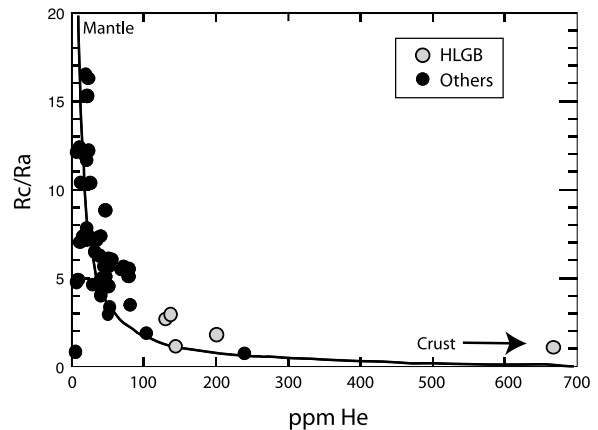


Figure 9. He isotopic composition versus He concentration (molar, in noncondensable gas) for Yellowstone fumaroles. Other Yellowstone samples are from Bergfeld et al. [2011]. Within the HLGB and throughout Yellowstone, increasing He concentrations are associated with the addition of crustal ^4He and low Rc/Ra . The curve represents binary mixing of gas with 10 ppm He and $\text{Rc}/\text{Ra} = 20$ (mantle) with a “crust” end-member of 1000 ppm He and Rc/Ra of 0.01. HLGB samples have among the highest concentrations of He measured at Yellowstone. Analytical uncertainties are smaller than the plot symbols.

(G8) is >300 times that of air and greater than that of most other HLGB samples.

5. Discussion

5.1. Origins of Fumaroles and Acid Pools

[34] Our multiple data sets are all consistent with a model whereby water flows out of the Yellowstone Caldera margin at the northwest end of the HLGB. Waters boil as they flow in the subsurface, emerging at different locations between the Upper Group to the northwest and the Rustic Group at the southeast end of HLGB. CO_2 discharge is concentrated in the Upper Group at the highest elevation and closest to the caldera. The isotopic compositions of steam samples are consistent with generation dominantly by boiling at temperatures between 150°C and 90°C (Figure 6), as calculated by using equations from Horita and Wesolowski [1994]. Fumarole gas contents are highest in the Upper Group and steadily decrease toward the southeast, consistent with lateral flow of subsurface thermal water, boiling, and progressive degassing. Moreover, the proportion of atmosphere-derived Ar, organic/light carbon, and crustal He increases toward the southeast (Figures 7, 8, and 9), consistent

with addition of new meteoric and crustal components during lateral flow.

[35] The more acidic waters have a genetic link to deep boiling waters, though their composition is very different than the neutral Cl waters. Rising steam condenses into shallow meteoric waters, transferring latent heat to create steaming ground and shallow muddy pools [Ellis and Mahon, 1977]. Acid is generated as thermophilic respiration and oxidation convert H₂S into sulfuric acid [Nordstrom et al., 2009]. The resulting isotopic composition of these acid waters implies prolonged evaporative concentration of D and ¹⁸O at low (<90°C) temperature (Figure 6). The acidic waters (e.g., W5) have cation ratios consistent with isochemical dissolution of rhyolite [Giggenbach and Glasby, 1977; Hedenquist et al., 1994]. Their low to negligible Cl concentrations (Figure 4) reflect their derivation from condensed steam mixed with shallow meteoric water. Chloride remains in the deep liquid phase during boiling [White, 1957].

5.2. Implications of Linear Trends in Neutral Cl Waters

[36] Given the hydrologic, geologic, chemical, and isotopic evidence for boiling, we can revisit Figure 5 and the demonstrated correlations among key solutes in the neutral Cl waters [Mazor and Thompson, 1982]. The least concentrated, near boiling temperature, neutral Cl waters at HLGB from our data set is W4, with 222 mg L⁻¹ Cl compared with a maximum of 350 mg L⁻¹ in W11. Data from previous studies also report a minimum Cl concentration for neutral to alkaline, near-boiling fluids around 230 mg L⁻¹. Assuming that Cl remains with the liquid during boiling, about 35% boiling could account for the increase in Cl concentration from (waters similar to) W4 to W11. A similar degree of boiling is implied by the increase in SiO₂. However, some of the trend exhibited in Figure 5 can certainly be attributed to mixing between a more concentrated “parent” fluid and low-solute meteoric water or steam condensate (Figure 5c). And plausibly, there could be a range of similar “parent fluids” that boil and mix with dilute water to produce the observed compositions and linear trend. More insight on the relative importance of mixing and boiling can be gained through mineral equilibria modeling and geothermometry.

5.3. Water and Gas Geothermometers

[37] Silica geothermometry relies on the enhanced solubility of quartz at elevated temperature

[Truesdell and Fournier, 1977]. Because the alkaline waters at HLGB are undersaturated with amorphous silica at emergence, the concentration of SiO₂ can be linked to the quartz-water equilibrium temperature at depth [Fournier, 1981]. Two end-member situations exist: one is where the water rises and cools conductively along its path, constantly losing heat to the wall rock. Such a condition is unlikely to exist beneath a geyser basin or in Yellowstone’s geothermal areas, where temperatures commonly increase with depth along or adjacent to the boiling curve [White et al., 1975]. Nevertheless, assuming conductive cooling, the SiO₂ content of sample W3, 369 mg L⁻¹, would imply an initial temperature of 226°C [Fournier, 1977; Truesdell and Fournier, 1977]. The other end-member assumes that the water cools adiabatically as it boils. Boiling along an adiabat increases the concentration of dissolved species, and the “quartz-adiabatic” geothermometer [Fournier, 1977], which corrects for this increase, yields a lower initial temperature (205°C for sample W3). Adiabatic boiling of 205°C water to its emergence at 93°C would generate 21% steam, implying an initial SiO₂ concentration of 292 mg L⁻¹.

[38] Other geothermometers provide similar results. The maximum temperature for a HLGB water from its Na/K ratio (14.5) is 187°C [Fournier, 1981]. Consideration of multiple samples to create a Cl-enthalpy plot [Truesdell and Fournier, 1977] yields an intercept with enthalpy corresponding to 210°C. Gases from White Gulch yield carbon isotope exchange temperatures [Horita, 2001] as high as 195°C (Table 2) with progressively lower temperatures calculated for down-gradient features as ¹³C values drop, and C₂/C₁ decreases, possibly due to introduction of low-temperature microbial CH₄ (section 5.8). Temperatures based on hydrogen-argon ratios [Giggenbach and Goguel, 1989] reach up to 194°C. In all, multiple geothermometers point to a temperature of 205°C ± 10°C for hot waters of the HLGB immediately prior to their adiabatic ascent, degassing, and emergence at the surface.

5.4. Modeling Mineral Solution Equilibria

[39] Subsurface temperatures can also be evaluated using calculations to estimate mineral saturation convergence [Reed and Spycher, 1984]. We used the computer code SOLMINEQ [Kharaka et al., 1988] to calculate mineral saturation indices (equivalent to the log *Q/K* of Reed and Spycher [1984]) for common rock-forming minerals in Yellowstone’s geothermal reservoirs. Sample W11

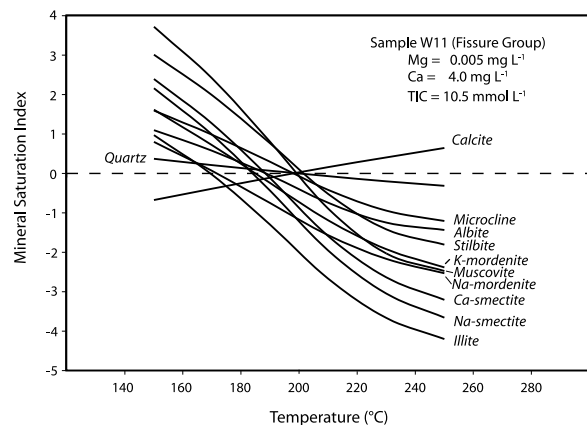


Figure 10. Mineral saturation index versus temperature calculated with the computer code SOLMINEQ [Kharaka *et al.*, 1988] for sample W11 in equilibrium with common minerals (pure end-members) from the Yellowstone hydrothermal system. The sample is predicted to saturate with a mineral where its curve crosses the saturation index of zero (horizontal dashed line). The model result represents a low-TIC fluid (10.5 mM), slightly adjusted for loss of Ca during upflow. The fluorite curve (not shown) is near horizontal and near saturation at all simulated temperatures.

(Fissure Group) with the highest chloride concentration was used as the basis for all calculations. The effects of two different concentrations of CO_2 were investigated, corresponding to the minimum and maximum values for diffuse emissions from section 4.4: 2 t d^{-1} as directly measured in diffuse degassing and 10 t d^{-1} as extrapolated to the entire Upper and Fissure Group areas. Given the thermal water discharge at HLGB of 61 L s^{-1} , a 2 t d^{-1} CO_2 efflux equates to a deep fluid that loses 8 mmol CO_2 on boiling; 10 t d^{-1} equates to loss of 40 mmol L^{-1} . Sample W11 contained about 2.5 mmol total inorganic carbon (TIC) at the surface, so the TIC in the starting parent fluid was set to 10.5 and 42.5 mmol to simulate the two CO_2 emission levels. Total alkalinity was “conserved” during boiling, as is customarily assumed, but concentrations of *all* species (including alkalinity) were reduced from measured concentrations in W11 to account for the steam lost during adiabatic boiling from an initial deep temperature to the ground surface temperature. In the calculations, temperatures increased from 150°C to 250°C in 20°C increments. Mineral saturation indices were plotted for primary and secondary minerals identified in Yellowstone drill cores in Lava Creek Tuff and overlying units [Honda and Muffler, 1970; Keith and Muffler, 1978]. Common alteration minerals in

the deepest, hottest parts of these drilled wells were quartz and cristobalite, various zeolites including mordenite, sheet silicates such as montmorillonite, illite, and celadonite and occasional calcite, feldspars and fluorite. The SOLMINEQ mineral database does not contain data for celadonite (a mica mineral), but the others are included.

[40] We calculated the saturation indices of quartz, zeolites including stilbite, K-mordenite and Na-mordenite, Ca- and Na-smectite, illite, microcline, albite, calcite, fluorite and other minerals. Initially, we used a very low Mg concentration (0.0002 mg L^{-1}), which was below the actual analytical detection limit of 0.005 mg L^{-1} . With 10.5 mmol TIC ($2 \text{ t d}^{-1} \text{ CO}_2$), most minerals were saturated (saturation index of 0) in the 170°C – 200°C range, with illite slightly lower at 163°C . The quartz saturation temperature was 201°C , with microcline (199°C) and muscovite (200°C) essentially matching quartz. Calcite and fluorite were undersaturated at all run temperatures. We speculate that precipitation of calcite during boiling and upflow has reduced Ca in the spring water creating the calculated undersaturation with the Ca-bearing minerals. Earlier workers [e.g., Bargar and Beeson, 1985] who sampled waters in research wells at Yellowstone also noted calcite undersaturation and attributed it to minor loss of CaCO_3 during boiling or sampling. If we revise the concentration to 4 mg L^{-1} Ca and raise Mg to the detection limit of 0.005 mg L^{-1} , calcite and fluorite achieve saturation near 200°C (Figure 10) and illite becomes saturated near 170°C . Overall, the simulations imply that the fluid equilibrated with known hydrothermal mineral assemblages in the subsurface at $190^\circ\text{C} \pm 15^\circ\text{C}$. The results are consistent with the idea that quartz preserves the best estimate of the deep temperature (201°C) [Fournier, 1981], while minor changes in cations during boiling and re-equilibration cause many of the other silicate minerals to indicate slightly lower equilibration temperatures and calcite and fluorite appear undersaturated [Mazor and Thompson, 1982].

[41] Model runs that accommodated the possibility of higher CO_2 emissions (10 t d^{-1}) required a lower pH fluid that drove all of the silicate minerals into undersaturation. Microcline and muscovite were close to saturation in the 160°C – 200°C range, but illite and stilbite were greatly undersaturated, as was calcite. By increasing Mg to the detection limit (0.005 mg L^{-1}), increasing alkalinity to 350 mg L^{-1} , and adding 15 mg L^{-1} Ca to balance the alkalinity, many of the important minerals attain saturation between 160°C and 200°C , though illite remained undersaturated. Overall, the results obtained

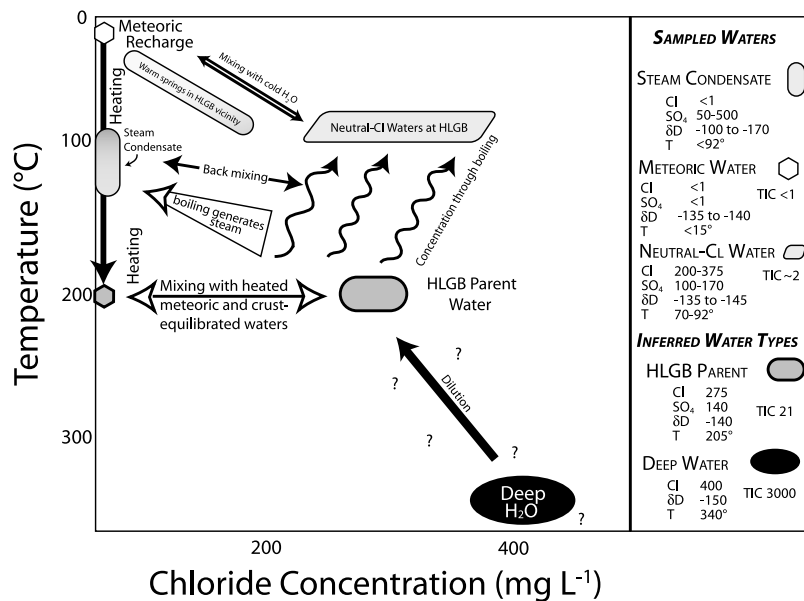


Figure 11. Schematic diagram of temperature versus Cl concentration, illustrating the end-member compositions involved in boiling and mixing during upflow beneath the Yellowstone Caldera and the Heart Lake Geyser Basin (HLGB). Shading gives qualitative indication of relative temperature. Zigzagging arrows show increases in Cl concentration for residual water during adiabatic ascent and boiling. Units of temperature are in °C, Cl and SO₄ are in mg L⁻¹, TIC is in mmol, and δD is in per mill VSMOW. Steam condensates are isotopically variable because of surface evaporation. Deep parent water is from Fournier [1989], Rye and Truesdell [2007], and Lowenstern and Hurwitz [2008]. All other data are from this study. Question marks reflect that the relation between any deep water and the HLGB parent water is speculative and beyond the scope of this paper.

with SOLMINEQ calculations were most consistent with the lower TIC fluid (10.5 mM, slightly adjusted for Ca loss) and equilibration temperatures close to 200°C.

5.5. Isotopic Systematics During Boiling

[42] The δD and δ¹⁸O ratios of HLGB waters are also consistent with subsurface and surface boiling to produce isotopic fractionation. As indicated in section 4.3, steam condensates from fumaroles imply boiling predominantly at temperatures below 150°C (Figure 6). The neutral Cl waters themselves form a collinear trend extending about 8‰ in δD from sample W4 to W3 (red dots in Figure 6). They are not displaced toward the isotopic compositions of the dilute/cold waters, so mixing with dilute waters clearly is not responsible for the primary trend. Instead, they are consistent with single-stage steam separation [Truesdell *et al.*, 1977] at 90°C, producing isotopically light steam (orange arrowhead in Figure 6) and heavy water (yellow arrowhead) when starting from a composition similar to sample S2 at 205°C ± 20°C from Gemery-Hill *et al.* [2007]. Truesdell *et al.* [1977] argued that waters from high-volume springs at Yellowstone would undergo adiabatic boiling, with the steam

rising along with the liquid to escape through single-stage degassing. In such a case, isotopic fractionation is maximized, and the overall trend dominated by low-temperature equilibration. Also possible, is multistage or continuous boiling, where the steam constantly separates from the rising liquid; however, this results in less isotopic fractionation than single-stage separation and is thus harder to reconcile with the considerable isotopic variation in the neutral Cl waters. Adiabatic boiling of 205°C water creates a steam fraction of 21%, or 79% residual liquid. This degree of boiling is certainly sufficient to account for the increase in solutes from ~300 mg L⁻¹ Cl to the most concentrated waters. The more dilute, isotopically light, near-boiling waters (e.g., W4) are most likely mixed with heated meteoric fluids or isotopically light steam condensate (Figure 11), though they may also be affected somewhat by boiling.

5.6. Mass Balance of Gas and Steam at Heart Lake Geyser Basin

[43] Fumarole samples from HLGB, especially those from the Rustic Group, are low in gas (%G << 1%). As shown in Figure 7, the gas contents of

HLGB samples overlap with those from other thermal areas at Yellowstone that discharge neutral Cl waters. Samples with low %G tend to have higher amounts of Ar, which are predominantly derived from air-saturated meteoric water (Figure 7 and Table 2). The CO₂ discharge from the region is also low. The measured net CO₂ flux (22.5 g m⁻² d⁻¹) in the steam-heated (acid sulfate) ground is about 5–10% that of Yellowstone's acid sulfate thermal areas that lack associated neutral Cl water discharge (e.g., Mud Volcano and Hot Spring Basin [Werner *et al.*, 2000, 2008]). Lowenstern and Hurwitz [2008] argued that the considerable CO₂ discharge from Yellowstone required that significant parts of the subsurface geothermal system were saturated with CO₂-bearing steam and that gas likely percolated through some regions without full dissolution in geothermal waters. The HLGB, in contrast, is one area where CO₂ discharge might readily be accounted for simply by boiling of the neutral Cl fluid.

[44] In section 4.4, we reported our measurement of 2.0 t d⁻¹ diffuse CO₂ flux from the Upper Group. Because we focused our measurements on those areas with the most obvious degassing, it is not likely that similar CO₂ efflux is found elsewhere at HLGB, though clearly 2.0 t d⁻¹ is a minimum value. An independent estimate of CO₂ flux can be derived from the total steam flux and the measured CO₂/H₂O of sampled fumaroles. Isenthalpic boiling of a 205°C liquid produces 1.66 × 10⁴ g s⁻¹ of steam to complement the 6.1 × 10⁴ g s⁻¹ (61 L s⁻¹) of discharged neutral Cl water (i.e., 21% boiling). The average %G in all six sampled fumaroles and frying pans at HLGB is 0.19 and corresponds to a CO₂/H₂O mass ratio of 0.0043. The 1.66 × 10⁴ g s⁻¹ of steam thereby yields a CO₂ emission rate of 72 g s⁻¹ or ~6 t d⁻¹. This value is intermediate between the actual measured diffuse flux and the extrapolation of the measured diffuse flux to the entire Fissure and Upper Groups (Table 3).

[45] Using this value for the total CO₂ emissions (72 g s⁻¹) relative to the total steam plus neutral Cl water emissions (77.3 L s⁻¹) converts to a CO₂ concentration of 21 ± 7 mmol in a HLGB parent fluid, prior to boiling (Table 3). This amount of CO₂ is readily soluble in 205°C waters at ~200 m depth, close to the hydrostatic boiling curve and represents ~230 kPa CO₂ pressure in that fluid. In summary, the steam and CO₂ discharge at the HLGB is consistent with migration, outflow and degassing of a boiling ~205°C ± 10°C thermal water. No extra source of CO₂, the primary gas, is required.

[46] Lowenstern and Hurwitz [2008] used similar reasoning to demonstrate that the CO₂ output from the Yellowstone Caldera and its immediate surroundings generally *does* require an extra source of gas, as the calculated CO₂ concentration for the bulk geothermal system is 3000 mmol or ~150 times greater than the molality implied by the diffuse gas flux and gas chemistry at HLGB. Waters at HLGB are instead consistent with boiling of a degassed fluid with low CO₂ that has migrated toward the caldera boundary and then boils as it ascends toward the surface (Figure 11). Plausibly, the HLGB waters originated from similar high-CO₂, deep waters that lost gas prior to entering the HLGB area; however, exploring such a relationship is beyond the scope of the present work.

5.7. Heat Discharge at Heart Lake Geyser Basin

[47] The heat budget of HLGB can be estimated from the initial enthalpy of the 77.3 L s⁻¹ of thermal water that leaves the HLGB as neutral Cl water and steam. Assuming that the water enters the Heart Lake area at 205°C, it transports 67.6 MW of heat, about 65% of which is carried by rising steam that condenses to form acid sulfate and other steam-heated areas (Table 3). To compare this with the method of Fournier *et al.* [1976], the thermal water and Cl ultimately would be derived from hotter, more Cl-rich thermal fluid from within the caldera (400 mg L⁻¹ and at 340°C). Because the deep parent of Fournier contains more Cl than our inferred water at HLGB (~300 mg L⁻¹), less mass is required and Fournier's method yields a similar heat flow of 72 MW, or about 1% of the estimated Yellowstone heat flow [Fournier *et al.*, 1976; Fournier, 1989; Hurwitz *et al.*, 2007]. In other words, either a local approach or Fournier's [1989] caldera-wide approach attributes similar amount of heat to the waters issued from HLGB.

5.8. Open-System Addition of Crustal Gases During Flow Beneath the HLGB

[48] Though steam and CO₂ discharge at HLGB can be reconciled with closed-system boiling and degassing of water that flows out of the Yellowstone Caldera, it is clear that some trace gas components are added to the hydrothermal fluid during flow beneath the Witch Creek drainage. As discussed above, the isotopic composition of carbon clearly changes between White Gulch and the more easterly (downhill) groups. CO₂ and CH₄ from the latter are lighter in ¹³C, potentially indicating

greater input from organic-sourced materials. The increase in C1/C2 along with the drop in $\delta^{13}\text{C}-\text{CH}_4$, however, is consistent with some addition of CH_4 from either bacterial or archaeal activity [Pohlman *et al.*, 2009]. It appears that shallow biological processes within and adjacent to HLGB springs and aquifers provide additional CH_4 and organic carbon that were added along the flow path. Presumably, this would also be evident in dissolved organic carbon in the sampled waters, which we did not attempt to measure.

[49] Values of $\delta^{13}\text{C}-\text{CH}_4$ correlate strongly with those of He isotopes (i.e., R_c/R_a). Rustic Group samples have much less indication of the magmatic signature that is so prevalent in many Yellowstone gases [Kennedy *et al.*, 1985; Bergfeld *et al.*, 2011]. Also, He, Ar, N₂, and CH₄ concentrations increase relative to the more soluble gas, CO₂ (Table 2). The increase in low-solubility, meteoric-derived gases such as Ar and N₂, as well as biogenic CH₄ and crustal He (with low R_c/R_a), requires that new gas is added along the flow path at the same time that the migrating thermal water is losing gas during subsurface boiling. The He-rich and radiogenic (⁴He) nature of the gas requires that at least part of it comes from warm crust-derived gases rather than those obtained solely from cold meteoric waters. Thus, the HLGB waters do exhibit some open-system addition of gas, notwithstanding their overall closed-system behavior during migration beneath the Witch Creek drainage.

6. Final Thoughts

[50] Yellowstone is remarkable for the chemical and isotopic heterogeneity of its thermal areas. Vast regions of the eastern part of the Yellowstone Caldera are characterized by acid sulfate terrain with little to no discharge of neutral Cl waters (e.g., Hot Springs Basin [Werner *et al.*, 2008]). To the west, basins within the Firehole River drainages contain little acid terrain but contain abundant springs of Cl-rich waters. Without the luxury of subsurface sampling, geochemists and hydrologists struggle to merge the disparate discharge, chemical, and isotopic data.

[51] Our study is novel in combining these various data types into a unified model for fluid migration, boiling, and mixing in a single thermal area at Yellowstone National Park. Figure 11 provides an overview of the types of waters at HLGB, their relative relationship, and pathways for mixing. Stable isotopes values, geothermometers, and solute

ratios are all consistent with adiabatic ascent and boiling of a $205^\circ\text{C} \pm 10^\circ\text{C}$ HLGB parent water that may be related by dilution to a more concentrated deep water present within the caldera [Fournier, 1989; Rye and Truesdell, 2007]. The diffuse CO₂ flux from HLGB and the range of gas contents (%G) of fumarolic gases is consistent with derivation of CO₂ by near closed-system degassing of the parent water during its adiabatic ascent and cooling. Unlike some other areas at Yellowstone where the gas flux far exceeds its solubility in the local geothermal waters, the modest CO₂ flux at HLGB can be readily exsolved from the coemitted, neutral Cl waters.

[52] As discussed by Hurwitz *et al.* [2007], Lowenstern and Hurwitz [2008], and Werner *et al.* [2008], the discharge of thermal water and gases is not so easily coupled at the gas-poor Firehole River basins or gas-rich Hot Spring Basin (with no neutral Cl water). The flow paths taken by their discharged fluids remain unclear, and the time periods required for circulation and discharge are unresolved. HLGB proves the exception to the rule; but its study yields insight that greater understanding of the Yellowstone hydrothermal system may be close at hand.

Acknowledgments

[53] Isotopic and chemical analyses were carried out in several USGS laboratories. We thank W. C. Pat Shanks (δD and $\delta^{18}\text{O}$), Kinga Revesz and Tyler Coplen ($\delta^{13}\text{C}$), Andy Hunt (³He/⁴He), and Mark Huebner (anions in water). We appreciate helpful reviews by E. Shock, B. McCleskey, and L. Shevenell. The USGS Volcano Hazards Program funded this work.

References

- Allen, E. T., and A. L. Day (1935) Hot springs of the Yellowstone National Park, *Carnegie Inst. Washington Publ.*, 466, 525 pp.
- Ball, J. W., D. K. Nordstrom, R. B. McCleskey, M. A. A. Schoonen, and Y. Xu (2001) Water-chemistry and on-site sulfur speciation data for selected springs in Yellowstone National Park, Wyoming, 1996–1998, *U.S. Geol. Surv. Open File Rep.*, 01–49, 47 pp.
- Bargar, K. E., and M. H. Beeson (1985), Hydrothermal alteration in research drill hole Y-3, Lower Geyser Basin, Yellowstone National Park, Wyoming, *U.S. Geol. Surv. Prof. Pap.*, 1054-C, 1–23.
- Bergfeld, D., J. B. Lowenstern, A. G. Hunt, W. C. P. Shanks III, and W. C. Evans (2011) Gas and isotope chemistry of thermal features from Yellowstone National Park, WY, *U.S. Geol. Surv. Sci. Invest. Rep.*, 2011–5012, 26 pp.
- Braunstein, D., and D. R. Lowe (2001), Relationship between spring and geyser activity and the deposition and morphology of high temperature (>73°C) siliceous sinter, Yellowstone National Park, Wyoming, U.S.A., *J. Sediment.*

- Res., 71, 747–763, doi:10.1306/2DC40965-0E47-11D7-8643000102C1865D.
- Brock, T. D. (1978), *Thermophilic Microorganisms and Life at High Temperatures*, 465 pp., Springer-Verlag, New York.
- Bryan, T. S. (2008), *The Geysers of Yellowstone*, 4th ed., 462 pp., Colo. Assoc. Univ. Press, Boulder.
- Chiodini, G., and L. Marini (1998), Hydrothermal gas equilibria, *Geochim. Cosmochim. Acta*, 62, 2673–2687, doi:10.1016/S0016-7037(98)00181-1.
- Chiodini, G., D. Granieri, R. Avino, S. Caliro, A. Costa, and C. Werner (2005), Carbon dioxide diffuse degassing and estimation of heat release from volcanic and hydrothermal systems, *J. Geophys. Res.*, 110, B08204, doi:10.1029/2004JB003542.
- Christiansen, R. L. (2001) The Quaternary and Pliocene Yellowstone Plateau volcanic field of Wyoming, Idaho, and Montana, *U.S. Geol. Surv. Prof. Pap.*, 729-G, 145 pp.
- Ellis, A. J., and W. A. J. Mahon (1977), *Chemistry and Geothermal Systems*, 392 pp., Academic, New York.
- Evans, W. C., D. Bergfeld, M. C. van Soest, M. A. Huebner, J. Fitzpatrick, and K. M. Revesz (2006), Geochemistry of low-temperature springs northwest of Yellowstone caldera: Seeking the link between seismicity, deformation, and fluid flow, *J. Volcanol. Geotherm. Res.*, 154, 169–180, doi:10.1016/j.jvolgeores.2006.01.001.
- Fahlquist, L., and C. Janik (1992) Procedures for collecting and analyzing gas samples from geothermal systems, *U.S. Geol. Surv. Open File Rep.*, 92–211, 19 pp.
- Fournier, R. O. (1977), Chemical geothermometers and mixing models for geothermal systems, *Geothermics*, 5, 41–50, doi:10.1016/0375-6505(77)90007-4.
- Fournier, R. O. (1981), Application of water geochemistry to geothermal exploration and reservoir engineering, in *Geothermal Systems: Principles and Case Histories*, edited by L. Ryback and L. J. P. Muffler, pp. 109–143, John Wiley, New York.
- Fournier, R. O. (1989), Geochemistry and dynamics of the Yellowstone National Park hydrothermal system, *Annu. Rev. Earth Planet. Sci.*, 17, 13–53, doi:10.1146/annurev.ea.17.050189.000305.
- Fournier, R. O., D. E. White, and A. H. Truesdell (1976), Convective heat flow in Yellowstone National Park, in *Proceedings: Second United Nations Symposium on the Development and Use of Geothermal Resources, San Francisco, California, USA, 20–29 May 1975*, pp. 731–739, U.S. Energy Res. and Dev. Admin., Washington, D. C.
- Gemery-Hill, P. A., W. C. Shanks III, L. S. Balistrieri, and G. K. Lee (2007), Geochemical data for selected rivers, lake waters, hydrothermal vents, and subaerial geysers in Yellowstone National Park, Wyoming and vicinity, 1996–2004, in *Integrated Geoscience Studies in the Greater Yellowstone area: Volcanic, Tectonic, and Hydrothermal Processes in the Yellowstone Geocosystem*, edited by L. A. Morgan et al., *U.S. Geol. Surv. Prof. Pap.*, 1717, 365–426.
- Giggenbach, W. F. (1980), Geothermal gas equilibria, *Geochim. Cosmochim. Acta*, 44, 2021–2032, doi:10.1016/0016-7037(80)90200-8.
- Giggenbach, W. F., and G. P. Glasby (1977) The influence of thermal activity on the trace metal distribution in marine sediments around White Island, New Zealand, *N. Z. Dep. Sci. Ind. Res. Bull.*, 218, 121–126.
- Giggenbach, W. F., and R. L. Goguel (1989) Collection and analysis of geothermal and volcanic water and gas discharges, *Rep. CD2401*, 81 pp., N. Z. Dep. of Sci. and Ind. Res., Wellington.
- Guidry, S. A., and H. S. Chafetz (2003), Depositional facies and diagenetic alteration in a relict siliceous hot-spring accumulation: Examples from Yellowstone National Park, U.S.A., *J. Sediment. Res.*, 71, 747–763.
- Hayden, F. V. (1883), *Twelfth Annual Report of the U.S. Geological Survey of the Territories, Part II, Yellowstone National Park Geology—Thermal Springs—Topography*, 503 pp., U.S. Geol. Surv., Washington, D. C.
- Hearn, E. H., B. M. Kennedy, and A. H. Truesdell (1990), Coupled variations in helium isotopes and fluid chemistry; Shoshone Geyser Basin, Yellowstone National Park, *Geochim. Cosmochim. Acta*, 54, 3103–3113, doi:10.1016/0016-7037(90)90126-6.
- Hedenquist, J. W. (1991), Boiling and dilution in the shallow portion of the Waiotapu geothermal system, New Zealand, *Geochim. Cosmochim. Acta*, 55, 2753–2765, doi:10.1016/0016-7037(91)90442-8.
- Hedenquist, J. W., M. Aoki, and H. Shinohara (1994), Flux of volatiles and ore-forming metals from the magmatic-hydrothermal system of Satsuma Iwojima volcano, *Geology*, 22, 585–588, doi:10.1130/0091-7613(1994)022<0585:FOVAOF>2.3.CO;2.
- Henley, R. W., and A. J. Ellis (1983), Geothermal systems ancient and modern, a geochemical review, *Earth Sci. Rev.*, 19, 1–50, doi:10.1016/0012-8252(83)90075-2.
- Honda, S., and L. J. P. Muffler (1970), Hydrothermal alteration in core from research drill hole Y-1, Upper Geyser Basin, Yellowstone National Park, Wyoming, *Am. Mineral.*, 55, 1714–1737.
- Horita, J. (2001), Carbon isotope exchange in the system CO₂-CH₄ at elevated temperatures, *Geochim. Cosmochim. Acta*, 65, 1907–1919, doi:10.1016/S0016-7037(01)00570-1.
- Horita, J., and D. J. Wesolowski (1994), Liquid–vapor fractionation of oxygen and hydrogen isotopes of water from the freezing to the critical temperature, *Geochim. Cosmochim. Acta*, 58, 3425–3437, doi:10.1016/0016-7037(94)90096-5.
- Hurwitz, S., J. B. Lowenstern, and H. Heasler (2007), Spatial and temporal geochemical trends in the hydrothermal system of Yellowstone National Park: Inferences from river solute fluxes, *J. Volcanol. Geotherm. Res.*, 162, 149–171, doi:10.1016/j.jvolgeores.2007.01.003.
- Hurwitz, S., W. C. Evans, and J. B. Lowenstern (2010), River solute fluxes reflecting active hydrothermal chemical weathering of the Yellowstone Plateau Volcanic Field, USA, *Chem. Geol.*, 276, 331–343, doi:10.1016/j.chemgeo.2010.07.001.
- Inskeep, W., D. K. Nordstrom, D. W. Mogk, A. W. Rodman, B. W. Foulke, N. Duraes, and M. Guzman (2010) Secondary minerals associated with geothermal features of Yellowstone National Park, in *Clays of Yellowstone National Park, CMS Workshop Lect.*, vol. 17, edited by P. A. Schroeder, pp. 24–51 Clay Miner. Soc., Chantilly, Va.
- Keith, T. E. C., and L. J. P. Muffler (1978), Minerals produced during cooling and hydrothermal alteration of ash flow tuff from Yellowstone drillhole Y-5, *J. Volcanol. Geotherm. Res.*, 3, 373–402, doi:10.1016/0377-0273(78)90044-6.
- Kennedy, B. M., M. A. Lynch, J. H. Reynolds, and S. P. Smith (1985), Intensive sampling of noble gases in fluids at Yellowstone: I. Early overview of the data; regional patterns, *Geochim. Cosmochim. Acta*, 49, 1251–1261, doi:10.1016/0016-7037(85)90014-6.
- Kharaka, Y. K., W. D. Gunter, P. K. Aggarwal, E. H. Perkins, and J. D. Dedraal (1988) SOLMINEQ.88, a computer

- program for geochemical modeling of water–rock interactions, *U.S. Geol. Surv. Water Res. Invest. Rep.*, 88–4227, 420 pp.
- Lewicki, J. L., D. Bergfeld, C. Cardellini, G. Chiodini, D. Granieri, N. Varley, and C. Werner (2005), Comparative soil CO₂ flux measurements and geostatistical estimation methods on Masaya volcano, Nicaragua, *Bull. Volcanol.*, 68, 76–90, doi:10.1007/s00445-005-0423-9.
- Lowenstern, J. B., and S. Hurwitz (2008), Monitoring a supervolcano in repose: Heat and volatile flux at the Yellowstone Caldera, *Elements*, 4(1), 35–40, doi:10.2113/GSELEMENTS.4.1.35.
- Mazor, E., and J. M. Thompson (1982), Evolution of geothermal fluids deduced from chemistry plots: Yellowstone National Park (U.S.A.), *J. Volcanol. Geotherm. Res.*, 12, 351–360, doi:10.1016/0377-0273(82)90034-8.
- Nordstrom, D. K., J. W. Ball, and R. B. McCleskey (2005) Ground water to surface water: Chemistry of thermal outflows in Yellowstone National Park, in *Geothermal Biology and Geochemistry in Yellowstone National Park*, edited by W. P. Inskeep and T. R. McDermott, pp. 73–94, Mont. State Univ. Publ., Bozeman.
- Nordstrom, D. K., R. B. McCleskey, and J. W. Ball (2009), Sulfur geochemistry of hydrothermal waters in Yellowstone National Park: IV Acid-sulfate waters, *Appl. Geochem.*, 24, 191–207, doi:10.1016/j.apgeochem.2008.11.019.
- Pohlman, J. W., M. Kaneko, V. B. Heuer, R. B. Coffin, and M. Whitticar (2009), Methane sources and production in the northern Cascadia margin gas hydrate system, *Earth Planet. Sci. Lett.*, 287, 504–512, doi:10.1016/j.epsl.2009.08.037.
- Reed, M., and N. Spycher (1984), Calculation of pH and mineral equilibria in hydrothermal waters with application to geothermometry and studies of boiling and dilution, *Geochim. Cosmochim. Acta*, 48, 1479–1492, doi:10.1016/0016-7037(84)90404-6.
- Rye, R. O., and A. H. Truesdell (2007), The question of recharge to the deep thermal reservoir underlying the geysers and hot springs of Yellowstone National Park, in *Integrated Geoscience Studies in the Greater Yellowstone Area: Volcanic, Tectonic, and Hydrothermal Processes in the Yellowstone Geosystem*, edited by L. A. Morgan et al., *U.S. Geol. Surv. Prof. Pap.*, 1717, 235–270.
- Schneider, V. R., and G. F. Smoot (1976), Development of a standard rating for the Price Pygmy current meter, *U.S. Geol. Surv. J. Res.*, 4, 293–297.
- Sheppard, D. S., A. H. Truesdell, and C. J. Janik (1992), Geothermal gas compositions in Yellowstone National Park, USA, *J. Volcanol. Geotherm. Res.*, 51, 79–93, doi:10.1016/0377-0273(92)90061-H.
- Theriot, E. C., S. C. Fritz, and R. E. Gresswell (1997), Long-term limnological data from the larger lakes of Yellowstone National Parks, *J. Arct. Alpine Res.*, 29, 304–314, doi:10.2307/1552145.
- Thompson, J. M., and J. M. DeMonge (1996) Chemical analyses of hot springs, pools, and geysers from Yellowstone National Park, Wyoming, and vicinity, 1980–1993, *U.S. Geol. Surv. Open File Rep.*, 96–0068, 66 pp.
- Thompson, J. M., T. S. Presser, R. B. Barnes, and D. B. Bird (1975), Chemical analysis of the waters of Yellowstone National Park, Wyoming from 1965 to 1973, *U.S. Geol. Surv. Open File Rep.*, 75–25, 59 pp.
- Truesdell, A. H., and R. O. Fournier (1977), Procedure for estimating the temperature of a hot water component in a mixed water using a plot of dissolved silica vs. enthalpy, *U.S. Geol. Surv. J. Res.*, 5, 49–52.
- Truesdell, A. H., and J. R. Hulston (1980) Isotopic evidence on environments of geothermal systems, in *Handbook of Environmental Isotope Geochemistry, vol. 1, The Terrestrial Environment*, edited by P. Fritz and J. C. Fontes, pp. 179–226, Elsevier, Amsterdam.
- Truesdell, A. H., M. Nathenson, and R. O. Rye (1977), The effects of subsurface boiling and dilution on the isotopic compositions of Yellowstone thermal waters, *J. Geophys. Res.*, 82, 3694–3704, doi:10.1029/JB082i026p03694.
- Werner, C., and S. Brantley (2003), CO₂ emissions from the Yellowstone volcanic system, *Geochem. Geophys. Geosyst.*, 4(7), 1061, doi:10.1029/2002GC000473.
- Werner, C., S. Brantley, and K. Boomer (2000), CO₂ emissions related to the Yellowstone volcanic system: 2. Statistical sampling, total degassing, and transport mechanisms, *J. Geophys. Res.*, 105, 10,831–10,846, doi:10.1029/1999JB900331.
- Werner, C., S. Hurwitz, W. C. Evans, J. B. Lowenstern, D. Bergfeld, H. Heasler, C. Jaworowski, and A. Hunt (2008), Volatile emissions and gas geochemistry of Hot Spring Basin, Yellowstone National Park, USA, *J. Volcanol. Geotherm. Res.*, 178, 751–762, doi:10.1016/j.jvolgeores.2008.09.016.
- White, D. E. (1957), Thermal waters of volcanic origin, *Geol. Soc. Am. Bull.*, 68, 1637–1658, doi:10.1130/0016-7606(1957)68[1637:TWOVO]2.0.CO;2.
- White, D. E., L. J. P. Muffler, and A. H. Truesdell (1971), Vapor-dominated hydrothermal systems compared with hot-water systems, *Econ. Geol.*, 66, 75–97, doi:10.2113/gsecongeo.66.1.75.
- White, D. E., R. O. Fournier, L. J. P. Muffler, and A. H. Truesdell (1975), Physical results of research drilling in thermal areas of Yellowstone National Park, Wyoming, *U.S. Geol. Surv. Prof. Pap.*, 892, 70 pp.
- Windman, T., N. Zolotova, F. Schwandner, and E. Shock (2007), Formate as an energy source for microbial metabolism in chemosynthetic zones of hydrothermal ecosystems, *Astrobiology*, 7, 873–890, doi:10.1089/ast.2007.0127.